Impact of resolution and air temperature on Large Eddy Simulation of mid-latitude summer time convection

Christopher Moseley[1], Ieda Pscheidt[2], Guido Cioni[1], and Rieke Heinze[1]

[1]Max Planck Institute for Meteorology, Hamburg, Germany
[2]University of Bonn, Germany

Correspondence: Christopher Moseley (christopher.moseley@mpimet.mpg.de)

Abstract. We analyze life cycles of summer time moist convection of a Large Eddy Simulation (LES) in a limited area setup over Germany. The goal is to assess the ability of the model to represent convective organization in space and time in comparison to radar data, and its sensitivity to daily mean surface air temperature. A continuous period of 36 days in May and June 2016, showing a considerable amount of convective rainfall which covers large parts of the domain on most of the

5 days, is simulated with a grid spacing of 625 m. Using convective organization indices, and a tracking algorithm for convective precipitation events, we find that an LES with 625 m grid spacing tends to underestimate the degree of convective organization, and shows a weaker sensitivity of heavy convective rainfall to temperature as suggested by the radar data. An analysis of three days within this period that are simulated with finer grid spacing of 312 m and 156 m showed, that a grid spacing at the 100 m scale has the potential to improve the simulated diurnal cycles of convection, the mean time evolution of single convective

10 events, and the degree of convective organization.

1 Introduction

An adequate representation of diurnal cycles of convection in atmospheric models is important for numerical weather predic-

15 tion and climate simulations, not only for the tropics (Ruppert and Hohenegger, 2018), but also for mid-latitude summertime convection (Pritchard and Somerville, 2009). For this purpose, cloud resolving models (CRM) are necessary, and are increasingly applied thanks to growing computational power. In the meanwhile, first global simulations with grid spacings between 7 km and 2.5 km have been performed (Stevens et al., 2019). This range is usually termed convection *permitting*, as not all relevant processes within convective cells are sufficiently resolved. In fact, in some of these models shallow convection is

20 parametrized in order to correct deficiencies in the simulation of smaller updrafts. Regional limited area models allow for even higher resolutions with grid spacings in the sub-kilometer range with Large Eddy Simulations (LES). Recently, selected diurnal cycles over a domain covering Germany and parts of neighbouring countries have been simulated in a realistic LES setup with

the model ICON-LEM, with grid spacing between 625 m and 156 m (Heinze et al., 2017) within the German funded project HD(CP)^2 ("High Definition Clouds and Precipitation for advancing Climate Prediction").

Previous studies have discussed the question which resolution is optimal for a good representation of the processes involved in deep convective updrafts. A semi-idealized study of days with precipitating convection by Petch et al. (2002) with grid spacings between 2 km and 125 m showed that the horizontal resolution should be at least one quarter of the sub-cloud layer depth, and that the best match with observational data was found only at the highest resolution. Similarly, a study by Bryan et al. (2003) showed that for an adequate simulation of a squall line using models with traditional LES closures, grid spacings of the order of 100 m are required. Further, it has been shown that for CRMs, model results strongly depend on the turbulence scheme (Panosetti et al., 2019). Besides horizontal resolution and the subgrid turbulence scheme, there are also other factors that impact the ability of CRMs to simulate convection, such as the microphysics scheme (Singh and O'Gorman, 2014), and the representation of the land surface.

The formation of strong convective precipitation events depends on several environmental conditions, like air temperature, surface fluxes, large scale forcing, and the ability of convection to organize. In the light of climate change, the sensitivity of precipitation extremes to warmer temperatures has been heavily discussed in the recent years in particular. The argument that the strongest events should increase at a rate of ca. 7% K^{-1} according to the thermodynamic Clausius-Clapeyron (CC) relation was put forward by Allen and Ingram (2002), and Trenberth et al. (2003). Observational evidence showed that even in mid-latitude regions, these rates can be even up to twice the CC rate (Lenderink and Van Meijgaard, 2008; Westra et al., 2014), which is predominantly the case for convective precipitation, while the stratiform precipitation type follows CC more closely (Berg et al., 2013). This indicates that beyond purely thermodynamic processes, also the dynamic component within convective clouds contributes to the intensification and has to be evaluated separately (Norris et al., 2019). CRMs should therefore also be able to simulate the time evolution of convective precipitation events and their interaction and organization among each other in a realistic way, to correctly represent their sensitivity to air temperature. This becomes increasingly difficult with decreasing model resolution, as Rasp et al. (2018) have shown that in principle subgrid cloud organization has to be included into stochastic cloud parametrizations. These parametrizations are particularly relevant at the above mentioned convection permitting scale, and at present assume a random cloud distribution within model grid cells.

To analyze the properties of convection and convective organization in model output and gridded observations like radar or satellite data, object oriented methods are increasingly applied. Besides simple mean values and percentiles of precipitation intensities, they provide information on the spatial distribution of sizes and shapes of precipitation objects. Furthermore, several indices that are based on these methods have been developed over the recent years, that are capable of quantifying the degree of organization of the convection cells in space (Senf et al., 2018; Pscheidt et al., 2019). Using a combination of several convective organization indices that we also apply in the present study, Pscheidt et al. (2019) have shown that convective precipitation cores and cloud-tops are organized most of the time over Germany.

However, the shortcoming of these methods is that they provide only information on the spatial distribution of convection objects, but not on their temporal evolution. Tracking methods are able to additionally capture the life cycles of the objects, and their interaction among each other. Several tracking methods for convective storms have been developed in the past, and

although they are based on similar ideas, they are specialized for different purposes, such as nowcasting thunderstorms (Dixon and Wiener, 1993; Hering et al., 2005; Kober and Tafferner, 2009; Wapler, 2017), studying the cloud life cycle statistics in shallow (Heus and Seifert, 2013; Heiblum et al., 2016), and deep convection (Lochbihler et al., 2017; Moseley et al., 2019), or even larger structures like mesoscale convective systems (Fiolleau and Roca, 2013).

5   In this study, we apply the tracking method by Moseley et al. (2019), which is suited to provide statistical information on the interaction of convective precipitation objects among each other in terms of merging and splitting. We analyze convective diurnal cycles simulated by the ICON-LEM with grid spacings in the sub-kilometer range, and assess the impact of horizontal resolution, and daily mean temperatures, on the simulated convection. This article is organized as follows: In section 2 we describe the ICON-LEM setup, the radar dataset that is used for evaluation, and the applied object oriented analysis methods.

10   In section 3, we compare the simulation results of three different model resolutions between 625 m and 165 m grid spacing, and in section 4 we analyze a continuous 36 day long simulation period with 625 m grid spacing. We discuss results in section 5, and conclude in section 6.

2   Data and methods

2.1   Model configuration

15   The simulations are performed with the unified modeling framework ICON which was run with the implemented LES physics package, in the following termed ICON-LEM ("ICON Large Eddy Model") (Dipankar et al., 2015). ICON is a non-hydrostatic new-generation model tailored to perform atmospheric simulations in different setups ranging from global climate reconstructions to limited-area nested configurations and idealized configurations. Different physics packages needed to parametrize sub-scale variability are adopted depending on the setup considered. ICON is used at the German Weather Service (DWD)

20   since 2015 to produce operational forecasts and has been successfully adopted as tool to improve our understanding of moist convection in many areas of the world (e.g. Klocke et al. (2017)).

In our work ICON-LEM is used in a limited area configuration to perform convection-explicit simulations over Germany. The model configuration follows very closely the description given in Heinze et al. (2017), to which the reader is referred for further details on the parametrizations employed. We only emphasize that turbulence is parametrized using a Smagorinsky model

25   (Dipankar et al., 2015), the land surface is described using the TERRA-ML model (Schrodin and Heise, 2002) and gravity waves (orographic and non-orographic) are not parametrized.

At the boundaries, ICON is forced by operational hourly analysis data by the previous operational NWP model COSMO-DE by the DWD, run with ca. 2.8 km grid spacing. The model output is interpolated to the ICON model grid with 625 m grid spacing, on which the model simulations are performed. Some days are further down scaled in a one-way nesting approach to

30   312 m, and 156 m grid spacings as done in Heinze et al. (2017). In this case, boundary conditions for each one of the two inner domains are taken from the relative outer domain (see Fig. 1).

2.2 Simulation period

We chose a period of 36 continuous days, beginning on May 26, 2016 and ending on June 20, 2016. This period includes an exceptional sequence of severe weather events producing heavy convective precipitation, 10 tornadoes and hail, which caused damages running into billions of Euros (Piper et al., 2016). The strongest events were concentrated between 26 and 29 May

5 2016 mostly over Southern Germany, while during the first day of June a Ω-blocking pattern over Europe prevented the typical westerly flow from reaching central Europe and enhanced local instability caused by diurnal surface heating and nocturnal cooling.

To reduce computational costs the entire 36-days period is simulated only on the outermost nest (domain 1) with 625 m grid spacing. The simulation is initialized on May 26, 2016 at 00:00 UTC and continuously run through June, 31 2016 00 UTC using

10 only the forcing from the boundary conditions provided by hourly analysis of the COSMO-DE data at the lateral boundaries of the outer domain. Local features, such as individual clouds or thunderstorms, are mostly the results of local forcing and thus may look different from the observed ones. Three days among this period are simulated with the additional nests with 312 m and 156 m grid spacing:

15 – **May 29, 2016**, was dominated mainly by wind from the South East, with relatively wide spread high level clouds that grew larger throughout the afternoon, and strong convection over the largest part of the domain. At night, a mesoscale convective system developed that covered most of southern Germany.

– **June 3, 2016**, was characterized by moderate Easterly wind in the Northern half of the domain with mainly clear sky in the morning and broken convective cloudiness in the afternoon. The Southern part of the domain was dominated by strong convective rainfall, beginning around noon.

20 – **June 6, 2016**, was characterized by weak Easterly winds, and a distinct diurnal cycle of convection with mainly clear sky in the morning, and convective cloudiness with a maximum in the afternoon over the largest part of the domain, associated by increasing high level cloudiness caused by stratiform outflow.

A more detailed description of the large scale situation in this period over Germany is given by Rasp et al. (2018), who analyzed the period between May 26 and June 9, 2016, in their study.

25 ## 2.3 Preparation of model and radar data

We use the RADOLAN RY C-Band weather radar composite provided by the German Weather Service (Bartels et al., 2004). This data product contains precipitation intensities derived from radar reflectivities on a grid of approximately $1 \times 1 \ km^2$. To achieve a fair comparison of all available data, we apply a conservative remapping to interpolate all model and radar data to a common latlon grid of $1 \times 1 \ km^2$. This implies that we also evaluate the model data on the three nests with 625 m, 312 m, and

30 156 m model grid spacing on the same target grid after interpolation.

As the radar data contain areas of missing values that vary in time when instruments were switched on and off, we mask out these areas also in the model data, to have a one to one comparison. In section 3, where we compare results of all three nests,
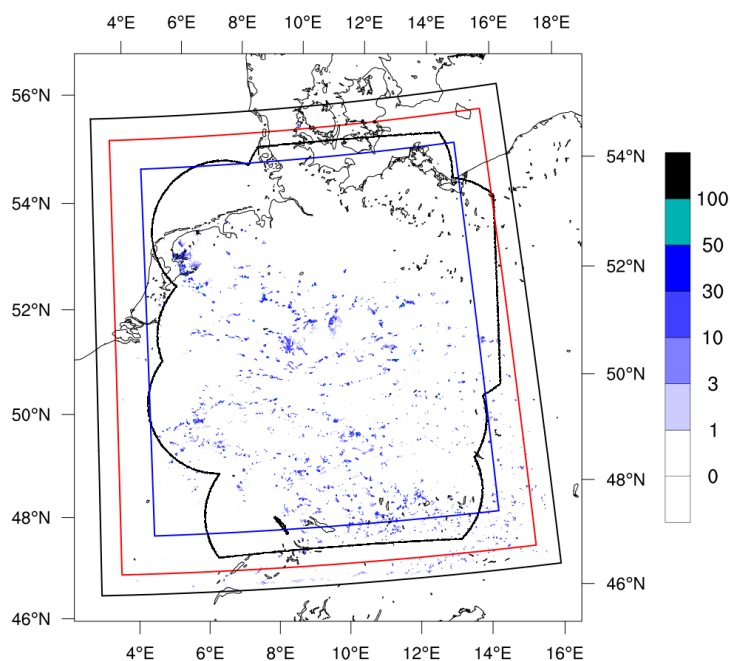
Figure 1. Simulation domain. The black frame shows the extent of the outer domain 1 with 625 m grid spacing, the red and blue frames show the nested domains 2 and 3 with 312 m, and 156 m grid spacing, respectively. The black contour shows the maximum extent of the RADOLAN dataset. Color shading shows the surface precipitation field on June 3, 2016, at 14:00 UTC, simulated on the outer domain with 625 m grid spacing, given in [mm h^{-1}].

we restrict the domain to the innermost nest with 156 m grid spacing as shown in Fig. 1. Elsewhere, where we analyze only the outer domain with 625 m grid spacing, we include the full domain size.

The temporal output interval of the model data is 2 min, while the radar data are available with a 5 min interval. Therefore, the modeled precipitation intensities have been linearly time interpolated to a 5 min interval.

5 **2.4 Indices of convective organization**

To investigate whether convective clouds tend to organize in space, we follow the approach used in Pscheidt et al. (2019): First, we detect signatures of convection in radar and model rain rates by applying a segmentation algorithm with a split-and-merge approach (Senf et al., 2018) with a threshold of 1 mm h^{-1}. In a second step, we compute commonly used organization indices for the radar observations and the simulation output. The organization indices are based on the characteristics of the 10 2D objects obtained from the segmentation algorithm. We employ three organization indices, namely the Simple Convective Aggregation Index (SCAI, (Tobin et al., 2012)), and the Convective Organization Potential (COP, (White et al., 2018)), which

are both based on all-neighbors distances, and the I_{org} index (Tompkins and Semie, 2017), which uses a nearest neighbor (NN) distance approach. SCAI is defined as

$$\mathrm{SCAI} = \frac{N D_0}{N_{max} L} 1000, \tag{1}$$

where N is the number of objects in the domain, D_0 is the geometric mean distance of the centroids between all possible pairs
5   of objects, N_{max} is the possible maximum number of objects that can exist in the domain, and L is the characteristic domain size. In this study, N_{max} is the total number of grid boxes in the domain, and L is the Southwest-Northeast distance in the domain. The degree of organization increases as the SCAI decreases.

COP considers the interaction potential between two objects $V(i,j) = (\sqrt{A(i)} + \sqrt{A(j)})/(d(i,j)\sqrt{\pi})$, where $A(i)$ is the area of object i and $d(i,j)$ is the Euclidean distance between the centroids of the objects i and j. COP is defined as

10   $$\mathrm{COP} = \frac{\sum_{i=1}^{N} \sum_{j=i+1}^{N} V(i,j)}{\frac{1}{2} N(N-1)}. \tag{2}$$

The degree of organization increases as COP increases.

Unlike SCAI and COP, the NN-based organization index I_{org} (Tompkins and Semie, 2017) is able to distinguish between the three types of spatial distribution: organized, regular, and random. In this approach, we treat objects as discs (similar to Nair et al., 1998), and compute the cumulative distribution function of the NN edge-to-edge distances (NNCDF) and compare
15   it to the NNCDF of theoretical randomly distributed objects over the same domain. The theoretical NNCDF is approximated by bootstrapping, in which a random number of objects with the observed size distribution is randomly placed over the domain (Weger et al., 1992; Nair et al., 1998). We perform 100 simulations and compare the observed NNCDF to the 100 theoretical NNCDFs in a graph. I_{org} is defined as the area below such a comparison curve (for more details see e.g. Pscheidt et al., 2019; Tompkins and Semie, 2017). From the 100 computed I_{org} indices we select the 2.5th and 97.5th percentiles to identify the
20   spatial distribution. The objects are organized in clusters when the 2.5th percentile is greater than 0.5, whereas they present a regular distribution in space when the 97.5th percentile is lower than 0.5. Otherwise, the scenario can not be differentiated from randomness.

In addition to the degree of convective organization, we also investigate the shape of the objects with the index I_{shape} defined as

25   $$I_{\mathrm{shape}} = \frac{1}{N} \sum_{i=1}^{N} s(i), \tag{3}$$

where $s(i) = P_{\mathrm{eq}}(i)/P(i)$ is the shape ratio, P(i) is the actual perimeter and $P_{\mathrm{eq}}(i) = \sqrt{4\pi A(i)}$ is the perimeter of an equivalent, area-equal disc of the object i. The perimeter P(i) is computed as the countour line through the centers of the border grid boxes of the objects (Benkrid and Crookes, Online; accessed 2017; van der Walt et al., 2014). I_{shape} ranges between 0 and 1 and indicates the predominant presence of linear shapes for the former and circular shapes for the latter. I_{shape} close to 0.5
30   indicates predominance of elliptical shapes.

2.5 Rain cell tracking

We apply the "Iterative raincell tracking" (IRT) algorithm to track life cycles of convective precipitation events in space and time (Moseley et al., 2019). In a first step, precipitation objects are detected for each time step individually, defined as connected areas over a given threshold chosen as $1\,\mathrm{mm\,h^{-1}}$ surface precipitation intensity which has proven to generate reasonable results,

5 and is in the order of the resolution threshold of the weather radar. For each object, the area, and the mean surface precipitation intensity averaged over this area is recorded. The algorithm checks for overlaps of each object with objects in the previous, and the subsequent time step, and records the concerning object identifiers. If an object overlaps with more than one object at the previous or subsequent time step, the two largest ones are recorded, others are ignored.

It sometimes happens that objects of subsequent time steps do not overlap although they belong to the same track, since they

10 are advected by mean background flow, especially if the time step is relatively large and the objects are small. To correct this artifact, in a second step a mean background advection field is diagnosed and the procedure is repeated by taking into account the displacements of the objects due to the advection field while checking for overlaps. This step has to be iterated until the object identification result converges.

In a third step, overlapping objects are combined to tracks. A fraction of the tracks have distinct life cycles, and do not

15 merge with others, nor split up into fragments. They are initiated as new emerging precipitation events and eventually vanish when surface precipitation ceases. We call these tracks *solitary*. Tracks that experience merging and splitting are recorded separately. We call these tracks *interacting*. A parameter, the so-called *termination sensitivity* Θ that takes values between 0 and 1, provides a criterion whether a merging or splitting event is recorded, or ignored. If $\Theta = 0$, then *every* merging and splitting event will lead to a termination of all involved tracks, and will be recorded as a tracks that interacts with its neighbours. In the

20 other extreme $\Theta = 1$, the largest object that experiences a merging or splitting event will always be continued and regarded as solitary, while the smaller involved tracks will be terminated and not be regarded as non-solitary. If Θ takes intermediate values, all participating tracks will only terminate, when they are of comparable size, otherwise the largest one will regarded as solitary, and the smaller one as interacting. For our analysis, we choose an intermediate value of $\Theta = 0.5$.

3 Impact of resolution

25 ### 3.1 Domain mean precipitation

To analyze the impact of resolution on the simulated life cycles of convection, we make use of the three days which have been simulated on three nests with 625 m (DOM01), 312 m (DOM02), and 156 m (DOM03) grid spacing. Fig. 2 shows the time series of the daily mean precipitation for each day for all three domains next to the radar data, averaged over all areas where radar data are available. While on May 29 the simulated precipitation amount on all three domains is very close to each other

30 and strongly mismatches the radar data, on the other two days in June 3 and 6 the time evolution of mean precipitation differs more strongly for the different resolution. On the latter two days, the match with RADOLAN is better for higher resolutions: The peak precipitation on the 625 m domain is larger, and is reached earlier than for the 312 m and 156 m nests. Both the
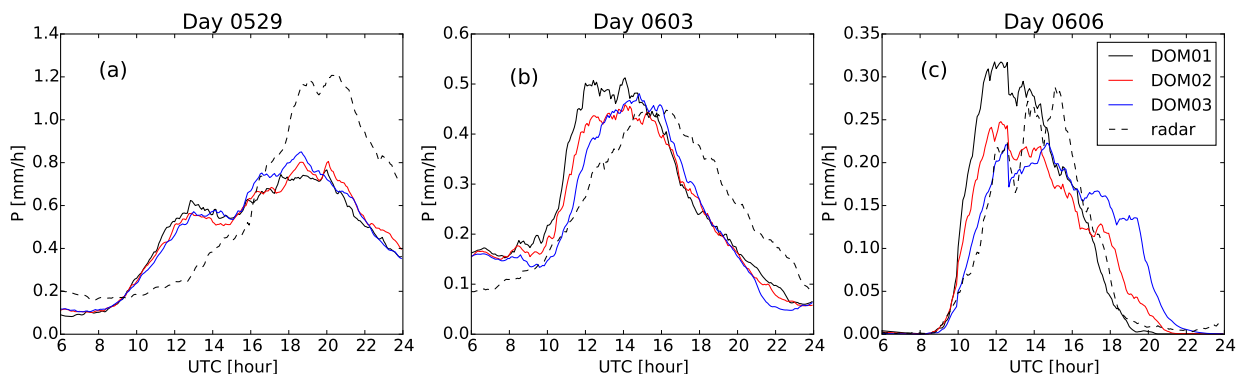
Figure 2. Time series of the mean precipitation intensity P, for the three days May 29 (a), June 3 (b), and June 6 (c), on all three domains with 625 m (DOM01), 312 m (DOM02), and 156 m (DOM03) grid spacing, and the RADOLAN derived precipitation intensity. Averaging was done over all grid boxes where radar data are available.

magnitude and the timing of the precipitation peak is closest to the radar data for the 312 m domain on June 3. On both June 3 and 6, the strong increase in precipitation around 10:00 UTC is steeper than in the radar data for 625 m, while the slope matches the radar data best for 156 m. However, on June 6 the decline of precipitation intensity in the late afternoon and evening hours appears too late.

3.2 Convective organization indices

A general convergence of the higher resolution nests to the RADOLAN data is not only found in the diurnal cycles of mean precipitation, but also in the organization indices that we have calculated on the three domains and the RADOLAN data, especially in SCAI and I_{shape} (Fig. 3). The analysis of SCAI reveals that on May 29 the radar objects are more clustered than the simulated ones (Fig. 3a), however, the finest nest is closest to RADOLAN. The 156 m nest also shows the best performance during June 6, when the degree of organization of observed objects is very well represented at 156 m (Fig. 3c). The situation is, however, different for June 3 (Fig. 3b). Before 12:00 UTC the finer nests represent best the degree of organization, whereas from 12:00 UTC until 18:00 UTC, the coarsest nest is in better agreement with radar. On all three days, there is a clear decrease in the degree of clustering with the nest's resolution, which seems to be due to an increase in the number of objects as the grid spacing increases.

The remaining organization indices show similar performances of the model simulations on May 29 and June 3, whereas for June 6 the results are somehow different (Fig. 3d–l). The COP index indicates more clustering of the radar objects than in the simulations in the course of both days, May 29 and June 3 mostly due to the smaller sizes of the simulated objects (not shown). A clustered distribution is also reinforced by I_{org} (Fig. 3g–i), indicating convective organization throughout the day with a slight decrease in the degree of clustering in the afternoon in agreement with SCAI and COP. The simulations represent I_{org} in all three grid spacings well and like COP, I_{org} does not reveal significant differences among the three grid spacings.
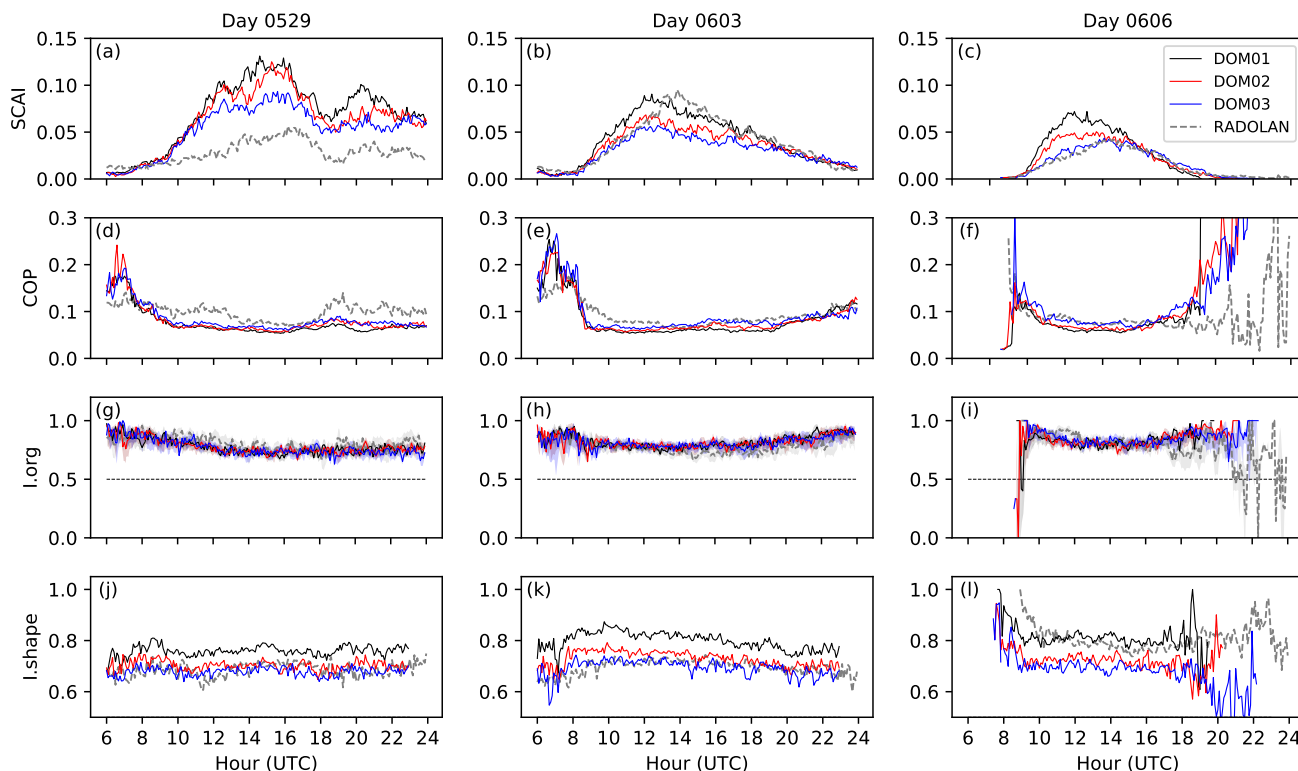
Figure 3. Convective organization indices SCAI (a-c), COP (d-f), median I_{org} (g-i) and I_{shape} (j-l) for the days May 29, June 3 and June 6, 2016, for the three nests with 625 m (DOM01), 312 m (DOM02), and 156 m (DOM03) grid spacing, and the RADOLAN data. Averaging was done over all grid boxes within the 165 m nest where radar data are available.

In contrast, the shape of the objects are best represented for the 156 m nest for the days May 29 and June 3, with decreasing performance for the coarser nests (Fig. 3j-k). For June 6, COP is in good agreement with radar between 09:00 UTC and 17:00 UTC for all three grid spacings (Fig. 3f). In the evening, however, the simulations with the finest nests reveal larger object sizes (not shown) than observed in radar leading to an overestimation of the degree of clustering. Besides, no objects are detected in

5   the 625 m nest after 19:00 UTC. The increased oscillation in the degree of clustering after 20:00 UTC seen in COP is reflected in I_{org}, and indicates spatial distributions varying between clustering and random distribution (Fig. 3i). For this day the 625 m nest is the closest to radar among the three grid spacings. Regarding the object's shapes, the coarsest nest shows the best performance for this day, though (Fig. 3l).

3.3   Track statistics

10   We now show that additional information on the temporal structure of the convective rainfall patterns are provided by the statistics of rain cell tracks. Therefore, we apply the tracking algorithm on the precipitation cells of model and RADOLAN

Table 1. Ratio of the number of tracks of given track types (solitary, tracks that involve only merging, tracks that involve only splitting, and tracks involving both merging and splitting), and the total amount of rainfall that they contribute, relative to the total number, and rainfall amount, respectively, of all tracks. Note that tracks that touch the domain boundaries are removed from the analysis. Fractions (in [%]), including all three 3-domain days, are given for all three domains with 625 m (DOM01), 312 m (DOM02), and 156 m (DOM03) grid spacing, and for the RADOLAN composite.

Ratio (number; amount) [%]	DOM01	DOM02	DOM03	RADOLAN
Solitary tracks	43.0; 9.4	32.7; 7.1	32.3; 4.2	31.5; 6.7
Involving only merging	25.4; 36.7	26.3; 27.7	26.7; 28.2	26.5; 26.7
Involving only splitting	28.5; 24.1	28.7; 25.4	27.7; 20.4	27.5; 34.2
Both merging and splitting	12.1; 29.7	12.3; 39.8	13.3; 47.2	14.5; 32.4

data (note that all data are evaluated on the domain of the innermost nest, and on the same grid), and build a single sample containing all tracks of the three days. We perform a separate analysis for solitary tracks ((i.e. tracks that do not merge or split), for tracks that involve only merging (i.e. tracks that either merge into others or are initiated by merging of other tracks, but that do not involve splitting), tracks that involve only splitting (i.e. tracks that split up, or tracks that are initiated as a fragment

5 of a splitting event), and tracks that involve both merging and splitting (i.e. tracks that either are initiated as a merging even, and split up later, or that are initiated as a fragment and later merge again with other tracks), see Table 1. Although less than 10% of the total rainfall is generated by solitary tracks (excluding drizzle below the threshold of 1 mm h^{-1}, and tracks that touch the boundaries), there is a strong variation of the contribution of solitary tracks to the total rainfall, namely 9.4%, 7.1%, 4.2%, indicating the tendency toward more organization with increasing resolution. For comparison, for RADOLAN we find

10 a fraction of 6.7%, which is between the model results of the 312 m and 156 m nest. The ratio of the *number* of solitary tracks is largest for the 625 m domain, while it is similar for the two finer nests and RADOLAN. The ratio of the number of tracks belonging to the three interacting tracks types is very similar for all nests and matches well with RADOLAN, but there are differences in the contribution to total rainfall among these types: There is a clear increase with resolution from 29.5% (for DOM1) to 47.2% for the type that experiences both merging and splitting. As this track type can be regarded as the one that

15 experiences the strongest interaction with neighbouring tracks, the high rainfall ratio falling onto this track type at the 156 m nest indicates a stronger impact of convective organization. However, for RADOLAN, this ratio is only 32.4% which is close to the coarse resolution result.

Even though solitary tracks contribute to less than 10% of the total precipitation, they are most suited for an analysis of the time evolution of convective rainfall events. Therefore, we have a closer look at the performance of the model to simulate

20 solitary track life cycles. Mean life cycle composits of the three 3-domain days, comparing model and RADOLAN tracks and conditioned on short (20–40 min), intermediate (50–70 min), and long (80–100 min) track durations, are shown in Fig. 4. The curves show that generally the mean peak intensities get lower for higher resolutions, while the largest jump is visible between 312 m and 156 m grid spacing (Fig. 4a–c). The match with RADOLAN intensities is best for the 156 m nest. The track sizes do not show an improvement with increasing resolution compared to the radar data: Sizes are smaller in the model data than in

RADOLAN, except for short duration tracks at the 625 m domain. In contrast to intensity, track maximum extents of the 625 m domain show a better match with RADOLAN, while the sizes of tracks of the 312 m and 156 m nests are clearly smaller (Fig. 5d–f). The rate of total precipitation produced by the solitary rainfall events (i.e. the spatial integral of precipitation intensity integrated over the object area) shown in Fig. 5g-i), however, shows that for intermediate and long duration tracks simulated
5   with 625 m grid spacing, the too large intensities are compensated by the too small intensities, resulting in a good match with RADOLAN, while rates are clearly too small for the finer nests. Only for the short duration tracks, the precipitation rate of the 156 m nest agrees with RADOLAN, while the coarse resolution produces too much precipitation.

We further visualize the statistics of the solitary track peak intensities, the maximal effective radii of the objects (where the effective radius is given as $r_i = \sqrt{A/\pi}$ with A being the object's area), and the total precipitation amount produced by the
10   tracks (given as the spatial integral over the area, and the temporal integral along the track duration, of the local intensity), in the box-and-whisker plots in Fig. 5. The solid curves in Fig. 5a show that in total there are more solitary tracks found in the model data than in RADOLAN, but for longer durations, curves for RADOLAN and the 156 m nest converge. The decreased number of longer lasting solitary tracks reflects the stronger organization at the high resolution domain, since stronger convective events are more likely to interact with neighbouring tracks. As already indicated by the life cycles in Fig. 4, we see that the median
15   of peak intensities is lowest for the finest resolution and shows a good match with RADOLAN, while peak intensities reach higher values for the 625 m domain. However, the spread in peak intensities is much higher for the RADOLAN data for longer duration tracks, while it is lowest for the 156 m nest, a feature that is not visible in the mean life cycles in Fig. 4. Further, Fig. 5b confirms that RADOLAN track maximum sizes are best matched with the coarse 625 m domain, while sizes are smaller at higher resolutions. The spread of the maximum size distribution is relatively narrow compared to intensities, and is similar
20   for all resolutions including the RADOLAN data. Not surprisingly, the resulting total amount of precipitation produced by the tracks (Fig. 5c) strongly increases with track duration. For tracks longer than 1 hour, the spread of the inner quartiles between model data and RADOLAN matches best for the 625 m domain, while the median matches better with the finer nests, although they show a clearly smaller spread.

To briefly summarize this section, both the convective organization indices and the rain cell tracking show that for the
25   higher resolution nests there is a stronger tendency of convection to organize, which generally provides a better match with RADOLAN data. Further, convective precipitation increases more rapidly at the onset of convection at 625 m grid spacing, compared to the finer resolutions, and the RADOLAN data. This can be seen both in the diurnal cycle of mean precipitation, and the life cycle composits of the solitary tracks. However, at 625 m grid spacing, too strong rainfall intensities for solitary tracks are compensated by smaller object sizes, such that the total rainfall amounts produced by the tracks are similar as in
30   RADOLAN.
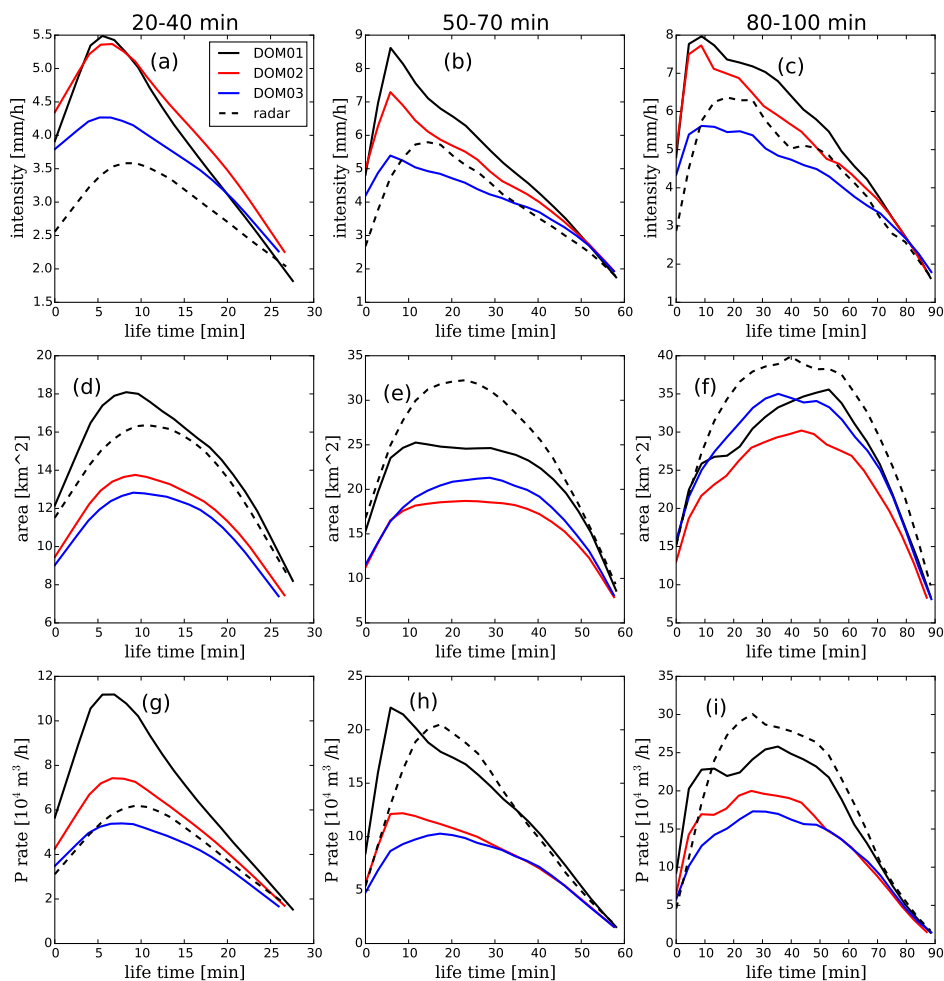
Figure 4. Life cycles of track composites (including the days May 29, June 3, and June 6) for solitary tracks of different track duration for model results on three domains with 625 m (DOM01), 312 m (DOM02), and 156 m (DOM03) grid spacings, and for radar results. Curves show mean track life cycles of area-mean precipitation intensity (a–c), area of precipitation objects (d–f), and rate of total precipitation (that is the areal integral of local precipitation intensity over the object extent) (g–i), conditioned on tracks with durations between 20–40 min (a,d,g), between 50–70 min (b,e,h), and between 80–100 min (c,f,i).
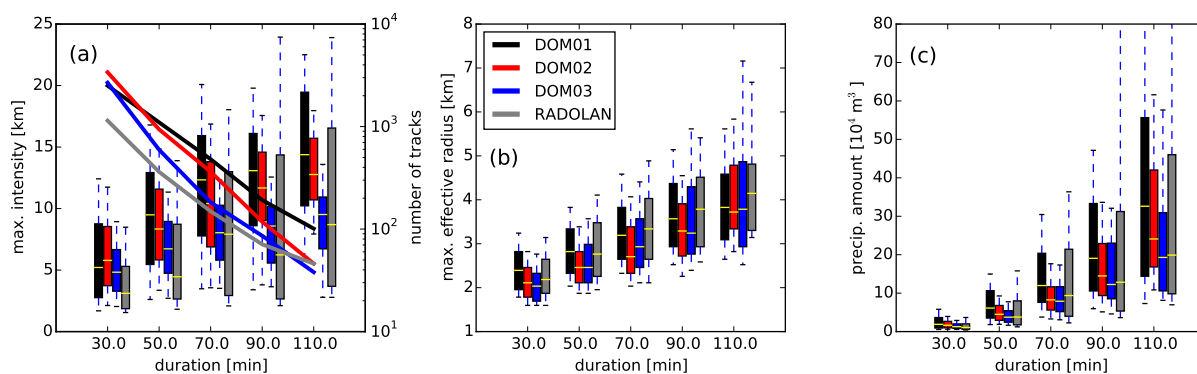
Figure 5. Box-and-whisker plots showing the statistics of solitary tracks, including the days May 29, June 3, and June 6 on all three domains with 625 m (DOM01), 312 m (DOM02), and 156 m (DOM03) grid spacing, and for the radar data. Values of track maximum intensity (a), track maximum effective radius (b), and total precipitation amount produced by the individual tracks (c), are conditioned on track duration ranging between 20 and 120 min, in 5 bins of 20 min width. Boxes indicate the 25th and 75th percentiles and the median (yellow bar), whiskers indicate the 10th and 90th percentiles. The number of tracks in each bin is indicated by the solid lines in panel (a) (note the logarithmic axis on the right).

4 Analysis of the continuous 36 days period with 625 m grid spacing

4.1 Mean diurnal cycles

In the previous section we argued that the ICON-LEM setup with 625 m grid spacing is sufficient to reasonably simulate typical convective summer days over Germany, although there may still be room for an added value at even higher resolutions.

5 We now discuss the continuous simulation period from May 26 until June 20, 2016, simulated with 625 m grid spacing. The simulated domain mean precipitation with the RADOLAN data for the full period is shown in Fig. 6. On some of the days we see an underestimation of simulated rainfall compared to RADOLAN, like on May 30, June 12, June 16, and in the 3-day period between June 23–25. However, there are few days where the precipitation intensity is slightly overestimated, like on June 19 and June 26. Another mismatch between model and radar data is that daily peak intensities tend to be reached 1–3

10 hours earlier in the model simulation compared to RADOLAN. This is particularly visible in the 6-days period June 3–8. This feature can be explained by the observation discussed in the section 3, where we argued that convection is triggered too fast in the 625 m LES simulation.

To confirm that the simulated 35-day convective period is long enough to show the intensification of convection with higher temperatures as discussed in the Introduction, and that it is also simulated with ICON-LEM and 625 m grid spacing, we perform

15 a separate analysis for selected cool and warm days. We calculate the domain mean temperature from the original COSMO-DE forcing data, and average over the time between 8:00 UTC and 20:00 UTC when daytime convection is expected. We hereby use the original COSMO-DE analysis data that provided the forcing, as we expect them to be closer to the actual temperatures than the temperatures simulated by ICON-LEM. We classify days below 16 °C daytime mean 2 m temperature as cool, and
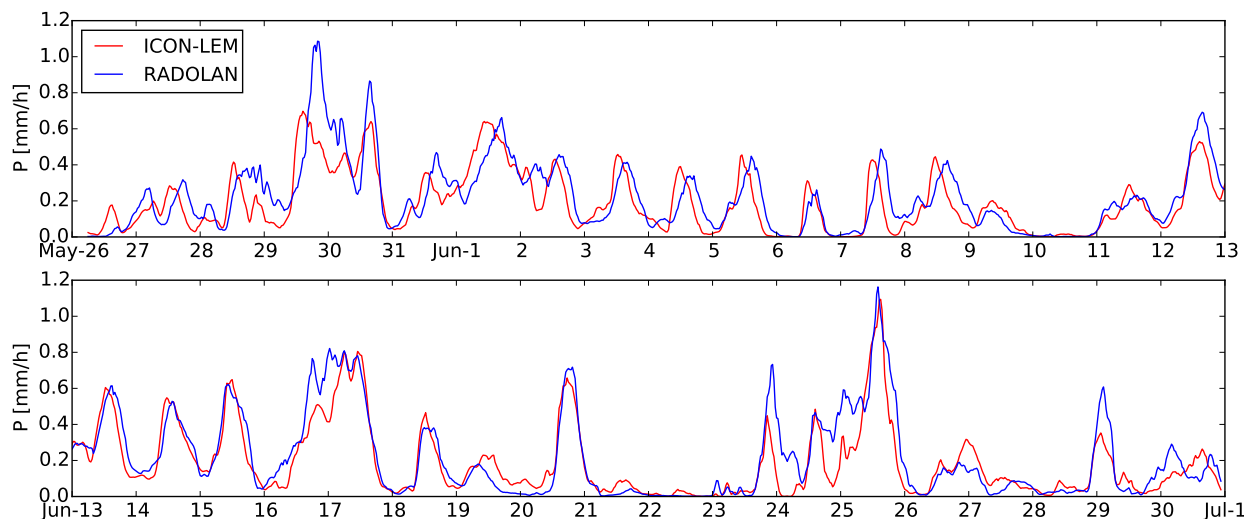
Figure 6. Time series of the mean precipitation intensity P for the 625 m grid spacing ICON-LEM simulation, and the RADOLAN derived precipitation intensity, for the full 36-days period from 26th May 2016 until 30th June 2016. Note that the time series was broken into the upper and the lower panel. Averaging was done over all grid boxes where radar data are available.

between 19 °C and 21 °C as warm. The two exceptionally warm days June 23 and June 24 with mean temperatures of 26.0 °C and 24.1 °C, respectively, are not included in the ensemble of warm days. Further, the day June 22 was removed from the classification due to the very low precipitation amount (otherwise it should have been classified as a warm day). An overview of the classified days can be seen in Table A1. In total, out of the 36 days of the simulation, we classify 6 days as cool, and 6
5 days as warm.

Mean diurnal cycles of several domain averaged quantities, including all 36 days, and conditioned on cool and warm days, are shown in Fig. 7. As already mentioned, the peak in mean precipitation (Fig. 7a) appears earlier in the model than in the RADOLAN data, and it is higher for the cold days than for the total mean of all days. For warm days, the peak is also slightly larger that for the total mean, although there is less precipitation in the afternoon hours after 15:00 UTC. The simulation
10 period is too short to significantly state if there is any direct correlation between the total amount of precipitation and the daily mean temperature. However, there is clear temperature dependence of the 99th percentile of precipitation intensity (Fig. 7b): In consistency with the CC argument mentioned in the Introduction, there is less (more) water vapor available in the atmosphere on cool (warm) days than on average (Fig. 7c), associated with lower (higher) extreme rainfall intensities. However, the differences in the 99th percentile of precipitation are more pronounced in the RADOLAN data, suggesting that the sensitivity of heavy
15 rainfall to temperature is underestimated by the model. Further, we see that cool (warm) days are associated with lower (higher) surface fluxes (Fig. 7d–f). Including the next warmer day above the 16 °C threshold to the cool days, and the next cooler day below the 19 °C threshold to the warm days as a sensitivity test, does not change this picture qualitatively (not shown).
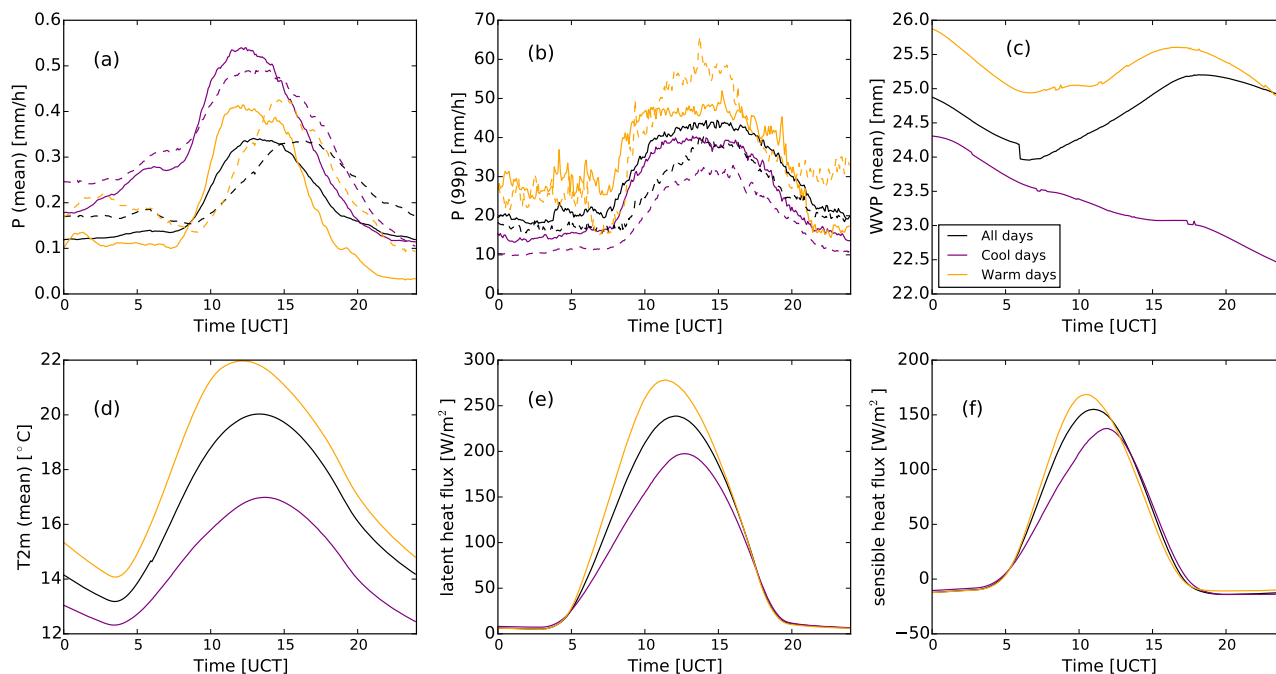
Figure 7. Diurnal cycles of mean precipitation intensity (a), 99th percentile of precipitation intensity (b), water vapor path (c), air temperature at 2 m (d), surface latent heat flux (e), and surface sensible heat flux (f), for all days, cold days, and warm days of the 36 day simulation with 625 m grid spacing. In panels (a) and (b), solid lines show simulation data, and dashed lines show RADOLAN data. Averaging was done over all grid boxes where radar data are available.

4.2 Diurnal cycles of convective organization indices

We calculate mean diurnal cycles of the convective organization indices SCAI, COP, I_{org}, and I_{shape}, for model and RADOLAN data of all 36 days, and conditioned on cool and warm days (Fig. 8). SCAI, COP and I_{org} indicate more organization in the morning and evening, when the objects present also a more elliptical shape (Fig. 8d). During the afternoon, when the convective

5 activity is more intense, there is a decrease in the degree of organization, with the shape of the objects tending towards a more circular one. ICON reproduces the diurnal cycle of I_{org} very well (Fig 8c). Although the variability of SCAI, COP and I_{shape} are captured by the model at 625 m grid spacing, it underestimates the degree of organization revealed by RADOLAN (Figs. 8a-b) and produces more rounded objects than the radar observations (Fig. 8d) especially in the afternoon, as was discussed in section 3.2.

10 For the 6 cool days, SCAI is in general larger, while COP is lower than the corresponding indices for the 35 days period (Fig. 8e,f), indicating the presence of more numerous and smaller objects. Although the degree of organization of these objects is weaker than for the full period (Fig. 8e–g), the variability in the shape (Fig. 8h) is similar to the larger period. In contrast to the cool days, during the 6 warm days, SCAI and COP show similar diurnal cycle to the 35 days period (Fig. 8i,j), revealing
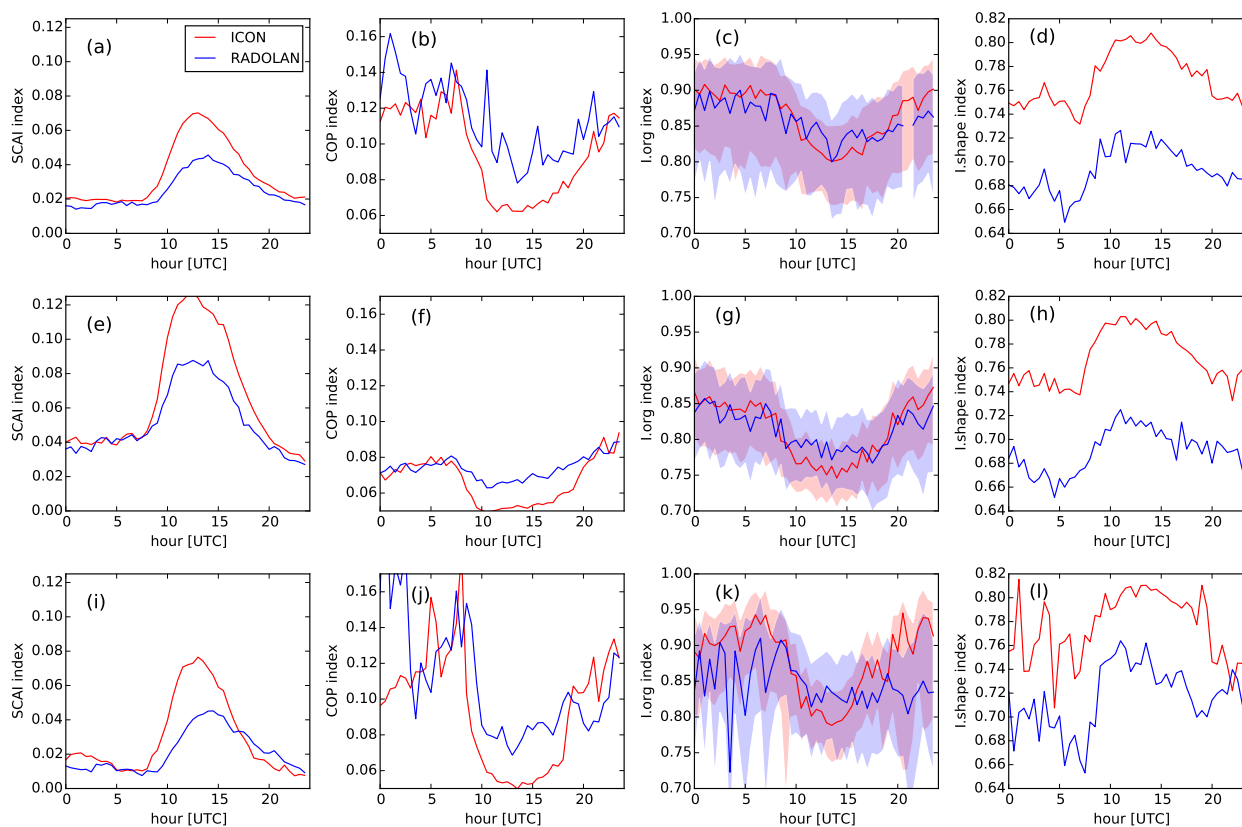
Figure 8. Mean diurnal cycles of the convective organization indices SCAI (a,e,i), COP (b,f,j), I_{org} (c,g,k; color shading shows the range between the 2.5th and 97.5th percentile as described in section 2.4), and I_{shape} (d,h,l), for all days (a–d), for cool days (e–h), and for warm days (i–l), for the model simulation with 625 m grid spacing, and for RADOLAN. Averaging was done over all grid boxes where radar data are available.

the presence of fewer and larger objects, which favours organization. I_{org} also indicates stronger degree of organization (Fig. 8k) in comparison with the cool days. Although I_{shape} is noisier on warm days, it also follows a similar behaviour (Fig. 8l) as seen during the longer period. Overall, the indices suggest a weaker degree of organization for the cool days compared to the 36-day average in both model and RADOLAN data. However, there is a less clear signal for the warm days compared to the average.

4.3 Track statistics

We have shown in section 3.3 that in addition to the four convective organization indices, the rain cell tracking result provides information on the degree of organization in the three different model resolutions. In this section we apply the rain cell tracking in a similar way on the 36-day continuous simulation with 625 m grid spacing with a separate analysis for the 6 cool days

Table 2. Ratio of the number of tracks of given track types (solitary, tracks that involve only merging, tracks that involve only splitting, and tracks involving both merging and splitting), and the total amount of rainfall that they contribute, relative to the total number, and rainfall amount, respectively, of all tracks. Tracks that touch the domain boundaries are removed from the analysis. Fractions (in [%]), including all 36 model days, and conditioned on only the cold, and the warm days, as defined in Table A1, are given for both the model simulation (M), and the RADOLAN composite (R).

Ratio (number; amount) [%]	All days (M)	Cool days (M)	Warm days (M)	All days (R)	Cool days (R)	Warm days (R)
Solitary tracks	38.8; 12.1	35.5; 11.9	39.1; 13.6	29.8; 5.1	26.5; 4.1	35.7; 8.4
Involving only merging	23.1; 27.0	23.8; 27.4	24.1; 28.7	27.8; 25.1	28.9; 25.1	26.9; 28.5
Involving only splitting	27.1; 26.5	28.6; 28.3	27.1; 25.6	27.6; 24.2	28.7; 23.1	25.2; 27.8
Both merging and splitting	11.0; 34.4	12.1; 32.4	9.7; 32.1	14.8; 25.6	15.8; 47.7	12.1; 35.3

and 6 warm days. Table 2 shows that there is a consistent trend in the ratio of both of the number and the total precipitation produced by solitary tracks, and that this trend is the same for model and RADOLAN data: There is a smaller fraction of solitary tracks on the cold days and a larger one on the warm days, compared to the full simulation period. Likewise, the solitary tracks contribute to a fraction of total rainfall that is smaller on cold days, but larger on warm days. At first glance, this

5   result seems to contradict our analysis of the three 3-domain days, where we argued that a *larger* contribution of solitary tracks corresponds to a *weaker* degree of organization: Instead, the organization indices in Fig. 8 show *weaker* organization on the cold days, although the contribution of solitary tracks is *smaller* meaning that a larger fraction of tracks is subject to merging or splitting events. However, it should be kept in mind that there was also more total precipitation in the analysis domain on the cool days, as compared to the total simulation period (Fig. 6), which is also reflected by the *total* number of tracks: While

10   there are on average 21533 solitary tracks per day for the full model period, the number of solitary tracks per day for the cold days was 33367 and therefore in total larger, while for the warm days there was a smaller number of only 20010 solitary tracks per day. For the RADOLAN data, these numbers were 8882 (all days), 17288 (cool days), and 9024 (warm days), respectively. Therefore, model and RADOLAN data agree on a larger *total number* of solitary tracks for the 6 cool days, in consistency with the hypothesis that a weaker organization on the cool days is associated with a larger number of non-interacting rain cells.

15   That the solitary track ratio with respect to the *total number* of all tracks is slightly smaller on the cool days, could be due to the fact that the larger number of precipitation objects (as indicated by the SCAI and COP indices) makes it more likely that neighboring objects interact with each other. This phenomenon was observed in the idealized LES study by Moseley et al. (2019) where model simulations with more convective rainfall and a larger number of rain cells showed a larger contribution of interacting rain cells to the total precipitation.

20   Similar as Fig. 5, the box-and-whisker plots in Fig. 9 show the statistics of maximum track intensities, maximum cell radii, and total precipitation amount of the solitary tracks. The solid lines in Fig. 9a–c show that the above mentioned larger number of solitary tracks per day of the cold days (Fig. 9b) is distributed over all track durations. Compared to the total ensemble of all 36 days, a smaller (larger) fraction of solitary tracks reach higher maximum intensities on cool (warm) days, and in consistency with the 99th percentile of rain intensities shown in Fig. 6b, there is a weaker temperaure sensitivity seen for the model data as
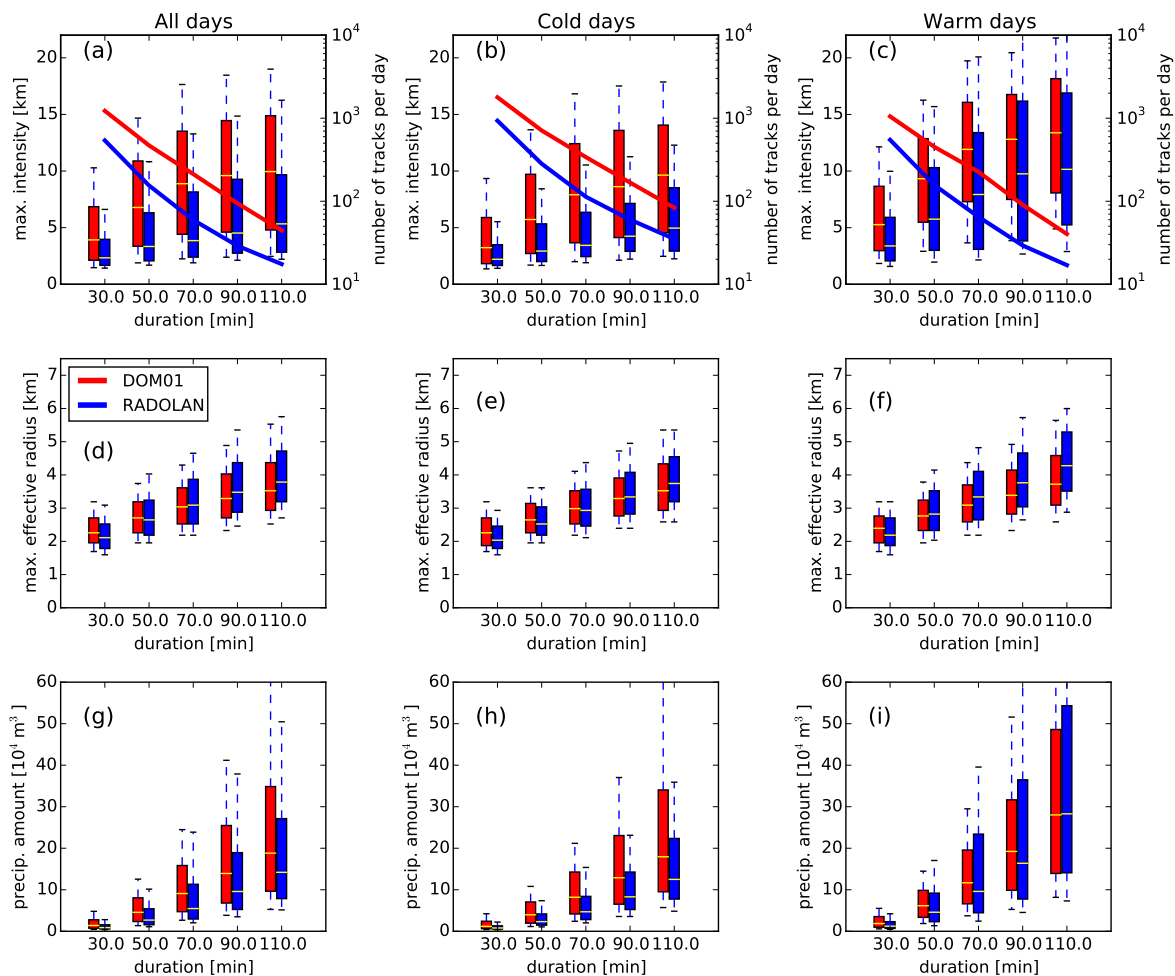
Figure 9. Box-and-whisker plots showing the statistics of solitary tracks for the whole 36-days period, for all (a,d,g), cold (b,e,h), and warm (c,f,l) days. Values of track maximum intensity (a–c), and track maximum effective radius (d–f), and total amount of precipitation produced by the individual tracks (g–l), are conditioned on track duration ranging between 20 and 120 min, in 5 bins of 20 min width. Boxes indicate the 25th and 75th percentiles and the median (red bar), whiskers indicate the 10th and 90th percentiles. The number of tracks in each bin is indicated by the solid lines in panels a–d (note the logarithmic axis on the right).

compared to RADOLAN. This intensification of the solitary tracks with temperature, especially for the longer durations tracks above 1 hour life time, can be seen even more clearly in the total amount of precipitation produced by the tracks (Fig. 9g–i). A dependence of the cell sizes reached by solitary tracks in temperature is less clear (Fig. 9d–f).

To briefly summarize the tracking result in this paragraph, we find that solitary tracks of comparable duration on warm
5 days can reach higher precipitation amounts on warm days as compared to cool days. This shows an intensification of solitary convective rain tracks with temperature. However, this intensification is found to be weaker for the model data compared to

RADOLAN. Furthermore, a larger number of solitary tracks on cool days in both model and RADOLAN data is consistent with a weaker degree of convective organization.

5 Discussion

We have evaluated the sensitivity of explicitly simulated convective precipitation with respect to horizontal resolution, and daily mean surface temperature. The impact of horizontal resolution is significant. Our study indicates that compared to the RADOLAN data, the diurnal cycles, life cycles, and degree of convective organization is simulated better at the innermost nest with 156 m horizontal grid spacing. This is in agreement with previous studies which argued that for a sufficient resolution of the processes within deep convective updrafts, models with grid spacing of the order of ca. 100 m are required (Petch et al., 2002; Bryan et al., 2003). At 625 m and to a smaller degree at 312 m grid spacing, convection tends to set in too rapidly, and many isolated deep convective cells are scattered over the domain. In contrast, at 156 m, we find a smoother onset of convective updrafts with lower peak intensities, and a stronger degree of organization with the tendency to form larger clusters, that in general show a better match with the radar data. Petch et al. (2002) argues that at coarser resolutions the models fail to compensate for the lack of resolved transport out of the sub-cloud layer, leading to a delayed spin-up of convection relative to that obtained in the better-resolved simulations. This delay in the spin-up might then lead to the too explosive convective initiation that we find in our analysis. An improved subgrid scheme might lead to more realistic results and a decreased sensitivity to resolution, while the Smagorinsky subgrid scheme used in our model seems to be not the optimal choice at 625 m grid spacing. An analysis of the impact of different turbulence schemes on the simulated convection is not covered here but should be left for future studies.

Similar as Pscheidt et al. (2019), we find in general a too large number of small clouds as indicated by the SCAI and COP indices in the model simulations, but in contrast to their findings we see a tendency towards less and larger objects at high resolution which we find more realistic as evaluated against the RADOLAN data. Further, similar to our study, Pscheidt et al. (2019) find that objects are more elliptic at higher resolution as indicated by the I_{shape} index. However, they find this to be less realistic as to compared to RADOLAN and satellite data, while in two of the three days that we analyzed, I_{shape} at the 156 m nest matches better with RADOLAN. Although Pscheidt et al. (2019) use the same model at the same resolutions, and partly the same observational data as in our study, they have analyze different model days. Thus, the reason for the discrepancies might be that differences among different model resolutions depend on synoptic situations, which indicates that a larger sample of model days is needed to confirm the hypothesis that convective organization is better simulated at 156 m grid spacing. However, our hypothesis is also supported by the tracking result which shows that there are less solitary tracks (which – in turn – means more interaction between tracks) at higher resolutions, which provides a better match to the RADOLAN data.

Our analysis of the continuous 36-day period shows that the sensitivity of convection to near-surface temperatures expected from theory is at least simulated qualitatively at ICON-LEM at 625 m grid spacing. A separate analysis of 6 cool (below 16°C) and 6 warm days (19–21°C) shows a consistent increase with temperature in the 99th percentile of precipitation intensity, as well as in the total amount of precipitation generated by solitary tracks. This finding is encouraging, since it confirms that

the increase of extreme precipitation with temperature can be represented with CRMs at the kilometer scale. However, in our simulation period the simulated increase from cool to warm days is smaller in magnitude than in the RADOLAN data. In addition to heavy precipitation intensities, We also find a temperature sensitivity of the convective precipitation indices: In particular, they show a weaker degree of organization for the cool days in both model and RADOLAN data. Although this is

5 consistent with a larger number of solitary tracks on the cool days, the *fraction* of solitary tracks is smaller on the cool days. This is probably due to the fact that although the degree of organization might be weaker, there was more total precipitation on the cool days in our simulation period, making an interaction of precipitation object more likely since they are on average closer together. A deeper investigation of the interaction between events may be left to a future study, and the idealized study by Moseley et al. (2016) suggests that interaction between cells might well be intensified with higher temperatures. Our study

10 also leaves the question open if higher resolution will lead to an improved simulation of the sensitivity of heavy rainfall and convective organization to temperature, as only three model days are available on the higher resolved nests. Given that the magnitude of the intensification of heavy rainfall with temperature has both a thermodynamic (based on the CC argument) and a dynamic aspect, and that thermodynamic processes can be expected to be rather independent of resolution, we can assume that it is mainly an insufficient representation of the dynamics within the convection cells that causes an underestimated

15 intensification at 625 m grid spacing.

In addition to these findings, we have shown that the Iterative Raincell Tracking method (IRT) is not only a useful tool to study the life cycles of isolated convective rain events (that is, solitary tracks), but it is also able to provide information on the convective organization in the model simulations and observational data. In general, a smaller total contribution of isolated cells to the total rainfall indicates that the tendency of convection to interact and form clusters is larger, since it means that a larger

20 fraction of tracks experiences merging and splitting. Therefore, our tracking result is consistent with the convective organization indices. However, as also stated by Rasp et al. (2018), these indices describe only the spatial structure of the convection, but neglect the temporal structures of convective memory, which is an import aspect for parametrizations. Therefore, there is the need for new types of indices that also involve information on the temporal evolution of convective organization. A further development of our tracking method may fill this gap, as it includes the time evolution of convection cells and therefore has

25 the potential to provide a more comprehensive description of the processes that happen when repeated merging of individual convection cells lead to large clusters, such as mesoscale convective systems, squall lines, and tropical cyclones.

6   Conclusions

Based on a 36 day long continuous simulation in May and June 2016, we have shown that ICON in a limited area setup over Germany and a grid spacing of 625 m is able to simulate an intensification of isolated convective rain cells with temperature,

30 which is qualitatively in agreement with the RADOLAN radar composite but to a smaller degree. Further, we find a weaker degree of organization especially on cooler days, which is reflected by the convective organization indices, but also by a larger number of non-interaction (solitary) rain cell tracks.

However, an analysis of the three days that are available on all three nests showed that the convective organization pattern is best simulated at the highest resolution with 156 m grid spacing. At the coarsest nest with 625 m grid spacing, we find that convective events are too strong at the beginning of their life cycles, that they are weaker organized, and that they show a weaker tendency to merge and form clusters. This indicates that not all processes in the convective updrafts are optimally resolved at this resolution. Overall our evaluation of the three model resolutions suggests that an increase of model resolution toward the 100 m scale has the potential to provide a more realistic simulation of convection.

Based on our finding that stronger convective organization is associated with a smaller number of non-interacting tracks and more merging and splitting events between objects, we propose the development of new convective organization indices that are capable of monitoring not only the spatial, but also the temporal evolution of the convective clustering process. Such indices could be based on existing tracking algorithms such as the IRT method that we applied within this study.

Code and data availability. Primary data and scripts used in the analysis that may be used for reproducing the authors' work will be stored in the DKRZ long term archive. (A permanent URL link can be provided after the manuscript is accepted.)

Appendix A: Overview of simulated days

Author contributions. R.H., G.C., and C.M. designed and performed the model simulations, C.M. performed the tracking analysis, I.P. calculated the convective organization indices. C.M. conceived the original idea and coordinated the analysis. All authors contributed to the manuscript.

Competing interests. There are no competing interests.

Acknowledgements. We thank the German Climate Computing Center (DKRZ) for providing computing resources and assistance with the performance of the ICON simulations. The Germany Weather Service (DWD) is acknowledged for providing the RADOLAN radar composite. We thank Sophia Schäfer for proof reading the manuscript and suggestions for improvement. We acknowledge funding through the German Federal Ministry of Education and Research for the project "HD(CP)^2 - High definition clouds and precipitation for advancing climate prediction" within the framework programme "Research for Sustainable Development (FONA)", under 01LK1506F.

Table A1. Mean 2-m temperature T and 10-m wind speed v for each day, averaged over COSMO analysis data between 8 and 20 UTC, and daily precipitation sums P_M from model output, and P_R from RADOLAN. In the temperature column, colors show days classified as cool (blue), warm (orange), and very warm (red). The days marked in yellow are simulated on three domains. The table on the right continues the left.

Mon–Day	T [$°C$]	P_M [mm]	P_R [mm]
05–26	16.9	1.58	0.80
05–27	17.7	3.50	3.88
05–28	18.9	3.46	4.71
05–29	18.2	8.32	11.11
05–30	17.4	9.11	10.98
05–31	17.5	3.93	5.06
06–01	17.2	10.48	9.35
06–02	17.1	5.09	7.43
06–03	18.1	4.7	4.63
06–04	19.5	3.07	3.59
06–05	20.0	3.28	4.55
06–06	20.5	1.72	1.49
06–07	20.7	2.28	3.47
06–08	17.8	3.67	5.21
06–09	16.5	1.72	1.56
06–10	17.3	0.14	0.12
06–11	16.4	2.96	3.68
06–12	15.9	7.01	8.96

Mon–Day	T [$°C$]	P_M [mm]	P_R [mm]
06–13	15.7	7.36	8.00
06–14	15.9	6.07	6.71
06–15	15.8	6.19	7.04
06–16	17.0	5.19	7.42
06–17	15.4	11.12	12.03
06–18	16.2	3.31	3.68
06–19	15.3	2.31	1.71
06–20	17.2	7.50	6.63
06–21	18.4	1.20	0.70
06–22	22.0	0.30	0.11
06–23	26.0	2.77	4.07
06–24	24.1	3.12	6.93
06–25	19.6	11.11	15.09
06–26	17.2	2.11	2.02
06–27	17.3	2.35	1.67
06–28	18.5	1.50	1.33
06–29	19.3	2.82	4.14
06–30	18.6	2.89	3.55

References

Allen, M. R. and Ingram, W. J.: Constraints on future changes in climate and the hydrologic cycle, Nature, 419, 224–232, 2002.

Bartels, H., Weigl, E., Reich, T., Lang, P., Wagner, A., Kohler, O., and Gerlach, N.: Projekt RADOLAN – Routineverfahren zur Online-Aneichung der Radarniederschlagsdaten mit Hilfe von automatischen Bodennierderschlagsstationen (Ombrometer) (in German), Technical Report, Deutscher Wetterdienst, Offenbach, Germany, 2004.

Benkrid, K. and Crookes, D.: Design and FPGA Implementation of a Perimeter Estimator, http://www.cs.qub.ac.uk/~d.crookes/webpubs/papers/perimeter.doc, Online; accessed 2017.

Berg, P., Moseley, C., and Haerter, J. O.: Strong increase in convective precipitation in response to higher temperatures, Nature Geoscience, 6, 181–185, 2013.

Bryan, G. H., Wyngaard, J. C., and Fritsch, J. M.: Resolution requirements for the simulation of deep moist convection, Monthly Weather Review, 131, 2394–2416,

10.5194/acp-2019-638
2019-08-20
Author(s) 2019. CC BY 4.0 License.

Dipankar, A., Stevens, B., Heinze, R., Moseley, C., Zängl, G., Giorgetta, M., and Brdar, S.: Large eddy simulation using the general circulation model ICON, Journal of Advances in Modeling Earth Systems, 7, 963–986, https://doi.org/10.1002/2015MS000431, https://agupubs.onlinelibrary.wiley.com/doi/abs/10.1002/2015MS000431, 2015.

Dixon, M. and Wiener, G.: TITAN: Thunderstorm Identification, Tracking, Analsyis, and Nowcasting – A Radar-based Methodology, J. Atmos. Oceanic Technol., 1993, 785–797, 1993.

Fiolleau, T. and Roca, R.: An Algorithm for the Detection and Tracking of Tropical Mesoscale Convective Systems Using Infrared Images From Geostationary Satellite, IEEE Transactions on Geoscience and Remote Sensing, 51, 4302–4315, https://doi.org/10.1109/TGRS.2012.2227762, 2013.

Heiblum, R. H., Altaratz, O., Koren, I., Feingold, G., Kostinski, A. B., Khain, A. P., Ovchinnikov, M., Fredj, E., Dagan, G., Pinto, L., Yaish, R., and Chen, Q.: Characterization of cumulus cloud fields using trajectories in the center of gravity versus water mass phase space: 1. Cloud tracking and phase space description, Journal of Geophysical Research: Atmospheres, 121, 6336–6355, https://doi.org/10.1002/2015JD024186, http://dx.doi.org/10.1002/2015JD024186, 2015JD024186, 2016.

Heinze, R., Dipankar, A., Henken, C. C., Moseley, C., Sourdeval, O., Trömel, S., Xie, X., Adamidis, P., Ament, F., Baars, H., Barthlott, C., Behrendt, A., Blahak, U., Bley, S., Brdar, S., Brueck, M., Crewell, S., Deneke, H., Di Girolamo, P., Evaristo, R., Fischer, J., Frank, C., Friederichs, P., Göcke, T., Gorges, K., Hande, L., Hanke, M., Hansen, A., Hege, H.-C., Hoose, C., Jahns, T., Kalthoff, N., Klocke, D., Kneifel, S., Knippertz, P., Kuhn, A., van Laar, T., Macke, A., Maurer, V., Mayer, B., Meyer, C. I., Muppa, S. K., Neggers, R. A. J., Orlandi, E., Pantillon, F., Pospichal, B., Röber, N., Scheck, L., Seifert, A., Seifert, P., Senf, F., Siligam, P., Simmer, C., Steinke, S., Stevens, B., Wapler, K., Weniger, M., Wulfmeyer, V., Zängl, G., Zhang, D., and Quaas, J.: Large-eddy simulations over Germany using ICON: a comprehensive evaluation, Quarterly Journal of the Royal Meteorological Society, 143, 69–100, https://doi.org/10.1002/qj.2947, https://rmets.onlinelibrary.wiley.com/doi/abs/10.1002/qj.2947, 2017.

Hering, A., Senesi, S., Ambrosetti, P., and Bernard-Bouissieres, I.: Nowcasting thunderstorms in complex cases using radar data., WWRP Symbosium on Nowcasting and Very Short Range Forecasting, September 5th - 9th 2005, Toulouse, 2.14, 2005.

Heus, T. and Seifert, A.: Automated tracking of shallow cumulus clouds in large domain, long duration large eddy simulations, Geoscientific Model Development, 6, 1261–1273, https://doi.org/10.5194/gmd-6-1261-2013, https://www.geosci-model-dev.net/6/1261/2013/, 2013.

Klocke, D., Brueck, M., Hohenegger, C., and Stevens, B.: Rediscovery of the doldrums in storm-resolving simulations over the tropical Atlantic, Nature Geoscience, 10, 891, https://doi.org/10.1038/s41561-017-0005-4, 2017.

Kober, K. and Tafferner, A.: Tracking and nowcasting of convective cells using remote sensing data from radar and satellite, Meteorologische Zeitschrift, 18, 75–84, https://doi.org/10.1127/0941-2948/2009/359, http://dx.doi.org/10.1127/0941-2948/2009/359, 2009.

Lenderink, G. and Van Meijgaard, E.: Increase in hourly precipitation extremes beyond expectations from temperature changes, Nature Geoscience, 1, 511–514, 2008.

Lochbihler, K., Lenderink, G., and Siebesma, A. P.: The spatial extent of rainfall events and its relation to precipitation scaling, Geophysical Research Letters, 44, 8629–8636, https://doi.org/10.1002/2017GL074857, http://dx.doi.org/10.1002/2017GL074857, 2017GL074857, 2017.

Moseley, C., Hohenegger, C., Berg, P., and Haerter, J. O.: Intensification of convective extremes driven by cloud - cloud interaction., Nature Geoscience, 9, 748–752, 2016.

Moseley, C., Henneberg, O., and Haerter, J. O.: A Statistical Model for Isolated Convective Precipitation Events, Journal of Advances in Modeling Earth Systems, 11, 360–375, https://doi.org/10.1029/2018MS001383, https://agupubs.onlinelibrary.wiley.com/doi/abs/10.1029/2018MS001383, 2019.

Nair, U., Weger, R., Kuo, K., and Welch, R.: Clustering, randomness, and regularity in cloud fields. 5. The nature of regular cumulus cloud fields, J.Geophys.Res., 103, 11 363–11 380, 1998.

Norris, J., Chen, G., and Neelin, J. D.: Thermodynamic versus Dynamic Controls on Extreme Precipitation in a Warming Climate from the Community Earth System Model Large Ensemble, Journal of Climate, 32, 1025–1045, https://doi.org/10.1175/JCLI-D-18-0302.1, https://doi.org/10.1175/JCLI-D-18-0302.1, 2019.

Panosetti, D., Schlemmer, L., and Schär, C.: Bulk and structural convergence at convection-resolving scales in real-case simulations of summertime moist convection over land, Quarterly Journal of the Royal Meteorological Society, pp. 1–17, https://doi.org/10.1002/qj.3502, https://rmets.onlinelibrary.wiley.com/doi/abs/10.1002/qj.3502, 2019.

Petch, J., Brown, A., and Gray, M.: The impact of horizontal resolution on the simulations of convective development over land, Quarterly Journal of the Royal Meteorological Society, 128, 2031–2044, https://doi.org/10.1256/003590002320603511, 2002.

Piper, D., Kunz, M., Ehmele, F., Mohr, S., Mühr, B., Kron, A., and Daniell, J.: Exceptional sequence of severe thunderstorms and related flash floods in May and June 2016 in Germany-Part 1: Meteorological background, Natural Hazards and Earth System Sciences, 16, 2835, https://doi.org/10.5194/nhess-16-2835-2016, 2016.

Pritchard, M. S. and Somerville, R. C. J.: Assessing the Diurnal Cycle of Precipitation in a Multi-Scale Climate Model, Journal of Advances in Modeling Earth Systems, 1, https://doi.org/10.3894/JAMES.2009.1.12, https://agupubs.onlinelibrary.wiley.com/doi/abs/10.3894/JAMES.2009.1.12, 2009.

Pscheidt, I., Senf, F., Heinze, R., Deneke, H., Trömel, S., and Hohenegger, C.: How Organized is Deep Convection over Germany?, accepted for publication in: Quarterly Journal of the Royal Meteorological Society, 0, 2019.

Rasp, S., Selz, T., and Craig, G. C.: Variability and Clustering of Midlatitude Summertime Convection: Testing the Craig and Cohen Theory in a Convection-Permitting Ensemble with Stochastic Boundary Layer Perturbations, Journal of the Atmospheric Sciences, 75, 691–706, https://doi.org/10.1175/JAS-D-17-0258.1, https://doi.org/10.1175/JAS-D-17-0258.1, 2018.

Ruppert, J. H. and Hohenegger, C.: Diurnal Circulation Adjustment and Organized Deep Convection, Journal of Climate, 31, 4899–4916, https://doi.org/10.1175/JCLI-D-17-0693.1, 2018.

Schrodin, R. and Heise, E.: A new multi-layer soil model, COSMO newsletter, 2, 149–151, 2002.

Senf, F., Klocke, D., and Brueck, M.: Size-Resolved Evaluation of Simulated Deep Tropical Convection, Monthly Weather review, 146, 2161–2182, 2018.

Singh, M. S. and O'Gorman, P. A.: Influence of microphysics on the scaling of precipitation extremes with temperature., Geophys. Res. Letts, 41, 6037–6077, 2014.

Stevens, B., Satoh, M., Auger, L., Biercamp, J., Bretherton, C. S., Chen, X., Dueben, P., Judt, F., Khairoutdinov, M., Klocke, D., Kodama, C., Kornblueh, L., Lin, S.-J., Putman, W. M., Shibuya, R., Neumann, P., Roeber, N., Vanniere, B., Vidale, P.-L., Wedi, N., and Zhou, L.: DYAMOND: The DYnamics of the Atmospheric general circulation Modeled On Non-hydrostatic Domains, Submitted, 2019.

Tobin, I., Bony, S., and Roca, R.: Observational evidence for Relationships between the Degree of Aggregation of Deep Convection, Water Vapor, Surface Fluxes, and Radiation, J.Climate, 25, 6885–6904, 2012.

Tompkins, A. and Semie, A.: Organization of tropical convection in low vertical wind shears: Role of updraft entrainment, J.Adv.Model.Earth Syst., 9, 1046–1068, https://doi.org/10.1002/2016MS000802, 2017.

Trenberth, K. E., Dai, A., Rasmussen, R. M., and Parsons, D. B.: The changing character of precipitation, B. Am. Meteorol. Soc., pp. 1,205–1,217, 2003.

van der Walt, S., Schönberger, J., Nunez-Iglesias, J., Boulogne, F., Warner, J., Yager, N., Gouillart, E., Yu, T., and and the scikit-image contributors: scikit-image: image processing in Python, https://doi.org/https://doi.org/10.7717/peerj.453, 2014.

Wapler, K.: The life-cycle of hailstorms: Lightning, radar reflectivity and rotation characteristics, Atmospheric Research, 193, 60–72, https://doi.org/10.1016/j.atmosres.2017.04.009, 2017.

5   Weger, R., Lee, J., Zhu, T., and Welch, R.: Clustering, Randomness and Regularity in Cloud Fields: 1. Theoretical Considerations, J.Geophys.Res., 97, 20,519–20,536, 1992.

Westra, S., Fowler, H., Evans, J., Alexander, L., Berg, P., Johnson, F., Kendon, E., Lenderink, G., and Roberts, N.: Future changes to the intensity and frequency of short-duration extreme rainfall, Reviews of Geophysics, 52, 522–555, 2014.

White, B., Buchanan, A., Birch, C., P.Stier, and Pearson, K.: Quantifying the Effects of Horizontal Grid Length and Parameterized Con-
10   vection on the Degree of Convective Organization Using a Metric of Potential for Convective Interation, J. Atmos. Sci., 75, 425–450, https://doi.org/10.1175/JAS-D-16-0307.1, 2018.